Inorg. Chem. **2008**, *47*, 2089−2097

$RE(AuAl_2)_nAl_2(Au_xSi_{1-x})_2$: A New Homologous Series of Quaternary Intermetallics Grown from Aluminum Flux

Susan E. Latturner[†] **and Mercouri G. Kanatzidis**[*,‡]

Department of Chemistry, Northwestern University, Evanston, Illinois 60208, and Department of Chemistry, Florida State University, Tallahassee, Florida 32306

Received September 12, 2007

The combination of early rare earth metals (La– to Gd and Yb), gold, and silicon in molten aluminum results in the formation of intermetallic compounds with four related structures, forming a new homologous series: $RE[AuAl_2]_nAl_2(Au_xSi_{1-x})_2$, with $x \approx 0.5$ for most of the compound and $n = 0$, 1, 2, and 3. Because of the highly reducing nature of the Al flux, rare earth oxides instead of metals can also be used in these reactions. These compounds grow as large plate-like crystals and have tetragonal structure types that can be viewed as intergrowths of the $BaAl_4$ structure and antifluorite-type $AuAl_2$ layers. $REAuAl_2Si$ materials form with the $BaAl_4$ structure type in space group *I*4/*mmm* (cell parameters for the La analogue are $a = 4.322(2)$ Å, $c = 10.750(4)$ Å, and $Z = 2$). $REAu_2Al_4Si$ forms in a new ordered superstructure of the KCu_4S_3 structure type, with space group *P*4/*nmm* and cell parameters of the La analogue of $a = 6.0973(6)$ Å, $c = 8.206(1)$ Å, and $Z = 2$. $REAu_3Al_6Si$ forms in a new *I*4/*mmm* symmetry structure type with cell parameters of $a = 4.2733(7)$ Å, $c = 22.582(5)$ Å, and $Z = 2$ for RE = Eu. The end member of the series, $REAu_4Al_8Si$, forms in space group *P*4/*mmm* with cell parameters for the Yb analogue of $a = 4.2294(4)$ Å, $c = 14.422(2)$ Å, and $Z = 1$. New intergrowth structures containing two different kinds of $AuAl_2$ layers were also observed. The magnetic behavior of all these compounds is derived from the RE ions. Comparison of the susceptibility data for the europium compounds indicates a switch from 3-D magnetic interactions to 2-D interactions as the size of the $AuAl_2$ layer increases. The Yb ions in $YbAu_{2.91}Al_6Si_{1.09}$ and $YbAu_{3.86}Al_8Si_{1.14}$ are divalent at high temperatures.

Introduction

The properties of modern industrial aluminum alloys are tailored by the addition of other elements such as transition metals and silicon to the aluminum. This results in the formation of adventitious intermetallic phases within the aluminum alloy.[1] Synthesis of intermetallics in an aluminum flux acts as a model for this aspect of aluminum alloys and also allows for the formation of relatively complex compounds not isolable using other techniques. The dissolution of elemental reactants in the flux renders them active well below their melting point, so synthesis can be carried out at lower temperatures, promoting the growth of new metastable or kinetically stabilized phases.[2] Exploratory synthesis in molten aluminum has produced many new multinary intermetallic compounds. New ternary phases resulting from the reaction of a tetrelide element (Si or Ge) and a transition metal or rare earth metal in excess aluminum include $Co_5Al_{14}Si_2$, $V_2Al_5Ge_5$, and $Ho_2Al_3Si_2$.[3] A combination of both a transition metal and a rare earth metal with a tetrelide in molten aluminum produces a variety of new quaternary intermetallic phases such as $Sm_2Ni(Ni_xSi_{1-x})Al_4Si_6$, $RE_4Fe_{2+x}Al_{7-x}Si_8$, $RE_8Ru_{12}Al_{49}Si_9(Al_xSi_{12-x})$, $SmNiAl_4Ge_2$, and $RE_2NiAl_4Ge_2$.[4] We have recently extended this work to explore the reactivity of third row transition metals such as gold in aluminum flux.

* To whom correspondence should be addressed. E-mail: m-kanatzidis@northwestern.edu.
† Florida State University.
‡ Northwestern University.

(1) (a) Suresh, S.; Mortensen, A.; Needleman, A. *Fundamentals of Metal-Matrix Composites*; Butterworth-Heinemann: Boston, 1993. (b) Mondolfo, L. F. *Aluminum Alloys: Structure and Properties*; Butterworth-Heinemann: Boston, 1979. (c) Gowri, S.; Samuel, F. H. *Metall. Mater. Trans. A* **1994**, *25*, 437–448.

(2) Kanatzidis, M. G.; Pottgen, R.; Jeitschko, W. *Angew. Chem., Int. Ed.* **2005**, *44*, 6996.

(3) (a) Wu, X. U.; Latturner, S. E.; Kanatzidis, M. G. *Inorg. Chem.* **2006**, *45*, 5358–5366. (b) Wu, X. U.; Bilc, D.; Mahanti, S. D.; Kanatzidis, M. G. *Chem. Commun.* **2004**, 1506–1507. (c) Chen, X. Z.; Sieve, B.; Henning, R.; Schultz, A. J.; Brazis, P.; Kannewurf, C. R.; Cowen, J. A.; Crosby, R.; Kanatzidis, M. G. *Angew. Chem., Int. Ed.* **1999**, *38*, 693–696.

10.1021/ic701799z CCC: $40.75
Published on Web 01/17/2008

Table 1. $RE[AuAl_2]_nAl_2(Au_xSi_{1-x})_2$ Compounds Synthesized in Aluminum Flux[a]

compound	space group	a (Å)	c (Å)	vol (Å^3)	R1/wR2	structure type
$LaAuAl_2Si$	$I4/mmm$	4.322(2)	10.750(4)	200.8(2)		$BaAl_4$ type
$CeAuAl_2Si$		4.250(2)	10.817(5)	195.4(3)		
$NdAuAl_2Si$		4.269(1)	10.848(3)	197.7(2)		
$EuAu_{0.6}Al_3Si_{0.4}$		4.3127(6)	11.208(2)	208.46(6)		
$LaAu_{1.96}Al_4Si_{1.04}$	$P4/nmm$	6.0973(6)	8.206(1)	305.06(6)	0.0236/0.0473	new; $REAu_2Al_4Si$ (supercell of KCu_4S_3)
$CeAu_{1.93}Al_4Si_{1.07}$		6.0697(4)	8.2003(7)	302.11(4)	0.0331/0.0760	
$PrAu_{1.94}Al_4Si_{1.06}$		6.044(1)	8.203(2)	299.7(1)	0.0253/0.0661	
$NdAu_{1.96}Al_4Si_{1.04}$		6.0271(6)	8.223(2)	298.71(7)	0.0258/0.0573	
$SmAu_2Al_4Si$		5.9981(8)	8.274(2)	297.68(8)		
$EuAu_{1.95}Al_4Si_{1.05}$	$P4/mmm$	4.3000(4)	8.337(1)	154.14(3)	0.0241/0.0584	KCu_4S_3
$NdAu_{2.81}Al_6Si_{1.19}$	$I4/mmm$	4.2492(3)	22.479(3)	405.88(7)	0.0267/0.0540	new; $REAu_3Al_6Si$
$EuAu_{2.58}Al_6Si_{1.42}$		4.2733(7)	22.582(5)	412.4(1)	0.0241/0.0576	
$YbAu_{2.91}Al_6Si_{1.09}$		4.2065(4)	22.893(3)	405.09(8)	0.0274/0.0574	
$CeAu_{3.91}Al_8Si_{1.09}$	$P4/mmm$	4.2577(8)	14.211(4)	257.6(1)	0.0288/0.0701	new; $REAu_4Al_8Si$
$PrAu_{3.86}Al_8Si_{1.14}$		4.2604(5)	14.224(2)	258.17(6)	0.0315/0.0748	
$NdAu_{3.93}Al_8Si_{1.07}$		4.252(1)	14.248(5)	257.6(1)		
$SmAu_{3.90}Al_8Si_{1.10}$		4.2360(6)	14.277(3)	256.18(7)	0.0420/0.1048	
$EuAu_{3.68}Al_8Si_{1.32}$		4.2689(3)	14.354(2)	261.58(4)	0.0317/0.0624	
$YbAu_{3.86}Al_8Si_{1.14}$		4.2294(4)	14.422(2)	257.97(5)	0.0240/0.0570	
$SmAu_{3.96}Al_8Si_{1.04}$	$I4/mmm$	5.9683(5)	28.594(3)	1018.5(1)	0.0326/0.0766	ordered $REAu_4Al_8Si$
$GdAu_{3.97}Al_8Si_{1.03}$		5.9788(7)	28.627(5)	1023.3(2)	0.0407/0.0969	
$Eu_2Au_{2.25}Al_6Si_{2.75}$	$I4/mmm$	4.2967(8)	27.871(8)	514.6(2)	0.0159/0.0361	Ce_2NiGa_{10}
$Gd_2Au_{4.93}Al_{10}Si_{2.07}$	$I4/mmm$	4.2256(4)	39.067(5)	697.6(1)	0.0355/0.0915	new

[a] For compounds with no R1/wR2 listing, only a partial data collection was carried out or the refinement was not complete/satisfactory.

Table 2. Crystallographic Collection Parameters of $LaAu_{1.96}Al_4Si_{1.04}$, $EuAu_{2.58}Al_6Si_{1.42}$, and $YbAu_{3.86}Al_8Si_{1.14}$

	$LaAu_{1.96}Al_4Si_{1.04}$	$EuAu_{2.58}Al_6Si_{1.42}$	$YbAu_{3.86}Al_8Si_{1.14}$
fw (g/mol)	662.10	861.12	1181.19
space group	$P4/nmm$	$I4/mmm$	$>P4/mmm$
a (Å)	6.0973(6)	4.2733(7)	4.2294(4)
c (Å)	8.206(1)	22.582(5)	14.422(2)
V (Å^3)	305.06(6)	412.38(14)	257.97(5)
Z	2	2	1
d_{calcd} (g/cm^3)	7.208	6.935	7.603
temp (K)	293	293	293
Radiation	Mo Kα	Mo Kα	Mo Kα
$2\theta_{max}$	74.95	74.79	74.66
index ranges	$-10 \le h \le 10$	$-7 \le h \le 7$	$-7 \le h \le 7$
	$-10 \le k \le 10$	$-7 \le k \le 7$	$-7 \le k \le 7$
	$-13 \le l \le 13$	$-38 \le l \le 38$	$-24 \le l \le 24$
reflns collected	4702	3266	3992
unique data/params	451/20	353/17	443/21
μ (mm^{-1})	27.74	30.70	64.42
R1/wR2 [$I > 2\sigma(I)$]	0.0236/0.0473	0.0241/0.0576	0.0240/0.0570
R1/wR2 (all data)	0.0282/0.0482	0.0250/0.0579	0.0270/0.0580
residual peaks (e/Å^3)	2.786, –3.964	3.473, –2.907	4.163, –2.969

In addition to its noble metal status and unusually high electronegativity,[5] gold is of great interest because of its extensive use in electronics applications. Gold wire–aluminum film connections are often found in semiconductor products, for instance. Studies of the binary intermetallics formed at these junctions have been crucial in optimizing the behavior of these components.[6,7] To facilitate the possible uses of rare earth aluminides and silicides in such applications, it is therefore relevant to investigate the behavior of gold in multinary intermetallic systems. In this work, the combination of gold, silicon, and early rare earth elements in molten aluminum produced four new and interrelated quaternary intermetallic structures. These compounds can be described as intergrowths of antifluorite-type $AuAl_2$ slabs and $BaAl_4$-type layers.[8] The group of structures can be expressed as a new homologous series, $RE[AuAl_2]_n$-$Al_2(Au_xSi_{1-x})_2$, with $n = 0$–3. The $n = 3$ member of this series, $REAu_4Al_8Si$, was previously discussed in a brief Communication.[9]

Experimental Procedures

Synthesis. In a nitrogen-filled glovebox, rare earth metals (Strem, 99.8%), Au (shavings from a 1 oz gold coin, 99.999%), Al pellets (Cerac, 99.99%), and Si powder (Cerac, 99.96%) were combined in a 1:1:10:5 molar ratio (0.14–0.18 g of RE, 0.197 g of Au, 0.270 g of Al, and 0.140 g of Si) in an alumina crucible. This was placed into a silica tube, which was sealed under a vacuum of 10^{-4} Torr. This sample was then heated to 1000 °C in 12 h, maintained at this temperature for 15 h, and then cooled to 860 °C in 20 h. It was annealed at 860 °C for 2 days and slowly cooled to room temperature over 3 days. The aluminum flux was removed by soaking the crucible in 5 M NaOH for 1 day. Other RE/Au/Al/Si elemental ratios (such as 1:2:10:5 and 1:3:10:2) were investigated in a similar fashion to determine the effect of changing reactant ratios on the mixture of products. A list of the products observed from these reactions is found in Table 1.

EDS Analysis. Selected single crystals were affixed to a SEM plate using carbon tape. Semiquantitative microprobe analysis of these samples was performed using a JEOL JSM-35C scanning electron microscope equipped with a Tracor Northern energy

(4) (a) Chen, X. Z.; Sportouch, S.; Sieve, B.; Brazis, P.; Kannewurf, C. R.; Cowen, J. A.; Patschke, R.; Kanatzidis, M. G. *Chem. Mater.* **1998**, *10*, 3202–3211. (b) Sieve, B.; Sportouch, S.; Chen, X. Z.; Cowen, J. A.; Brazis, P.; Kannewurf, C. R.; Papaefthymiou, V.; Kanatzidis, M. G. *Chem. Mater.* **2001**, *13*, 273–283. (c) Sieve, B.; Chen, X. Z.; Henning, R.; Brazis, P.; Kannewurf, C. R.; Cowen, J. A.; Schultz, A. J.; Kanatzidis, M. G. *J. Am. Chem. Soc.* **2001**, *123*, 7040–7047. (d) Sieve, B.; Chen, X. Z.; Cowen, J. A.; Larson, P.; Mahanti, S. D.; Kanatzidis, M. G. *Chem. Mater.* **1999**, *11*, 2451–2455. (e) Sieve, B.; Trikalitis, P. N.; Kanatzidis, M. G. *Z. Anorg. Allg. Chem.* **2002**, *628*, 1568–1574.

(5) Lee, J. D. *Concise Inorganic Chemistry*, 4th ed.; Chapman and Hall: London, 1991; Ch. 27 and references therein.

(6) (a) Kato, H. *Jpn. J. Appl. Phys.* **1986**, *25*, 934–935. (b) Mori, M.; Fukuda, Y.; Kizaki, Y.; Iida, A.; Saito, M. *Electron. Commun. Jpn.—Electronics* **1999**, *82*, 11–20.

(7) (a) Philofsky, E. *Solid-State Electron.* **1970**, *13*, 1391–1399. (b) Selikson, B.; Longo, T. A. *Proc. IEEE* **196452**, 1638.

(8) Villars, P. *Pearson's Handbook, Desk Edition, Crystallographic Data for Intermetallic Phases*; ASM International: Material Park, OH, 1997.

(9) Latturner, S. E.; Kanatzidis, M. G. *Chem. Commun.* **2003**, 2340–2341.

Table 3. Atomic Positions and Isotropic Thermal Parameters for $LaAu_{1.96}Al_4Si_{1.04}$[a]

atom	Wyckoff site	*x*	*y*	*z*	U_{eq}	occ
La	2b	0.75	0.25	0.5	0.005(1)	1
Au(1)/Si(1)	2c	0.25	0.25	0.3478(1)	0.005(1)	0.948(4)/0.052(4)
Si(2)/Au(2)	2c	0.25	0.25	0.6481(4)	0.004(1)	0.988(4)/0.012(4)
Au(3)	2a	0.75	0.25	0	0.004(1)	1
Al(1)	8j	0.0010(2)	0.0010(2)	0.1764(2)	0.006(1)	1

[a] In this and subsequent tables, U_{eq} is defined as 1/3 of the trace of the orthogonalized U_{ij} tensor.

Table 4. Atomic Positions and Isotropic Thermal Parameters for $EuAu_{2.58}Al_6Si_{1.42}$

atom	Wyckoff site	*x*	*y*	*z*	U_{eq}	occ
Eu	2a	0	0	0	0.007(1)	1
Au(1)/Si(1)	4e	0	0	0.4451(1)	0.006(1)	0.288(3)/0.712(3)
Au(2)	4e	0	0	0.1840(1)	0.005(1)	1
Al(1)	8g	0	0.5	0.1195(1)	0.007(1)	1
Al(2)	4d	0	0.5	0.25	0.006(1)	1

Table 5. Atomic Positions and Isotropic Thermal Parameters for $YbAu_{3.86}Al_8Si_{1.14}$

atom	site	*x*	*y*	*z*	U_{eq}	occ
Yb	1a	0	0	0	0.006(1)	1
Au(1)/Si(1)	2h	0.5	0.5	0.0866(1)	0.005(1)	0.432(3)/0.568(3)
Au(2)	2g	0	0	0.2896(1)	0.004(1)	1
Au(3)	1d	0.5	0.5	0.5	0.004(1)	1
Al(1)	4i	0	0.5	0.1881(2)	0.006(1)	1
Al(2)	4i	0.5	0	0.3952(2)	0.006(1)	1

Table 6. Representative Bond Length Ranges (Å). E.s.d. < 0.009 Å.

bond	$REAu_2Al_4Si$	$REAu_3Al_6Si$	$REAu_4Al_8Si$
RE–(Au/Si)	3.237–3.295	3.214–3.266	3.217–3.272
(Au/Si)–(Au/Si)	2.417–2.510	2.437–2.478	2.414–2.526
(Au/Si)–Al(1)	2.552–2.599	2.566–2.587	2.563–2.595
Al(1)–Au(2)	2.586–2.601	2.582–2.587	2.573–2.587
Au(2)–Al(2)		2.589–2.605	2.594–2.607
Al(2)–Au(3)			2.598–2.600

dispersive spectroscopy (EDS) detector. Data were acquired using a 20 kV accelerating voltage and an accumulation time of 50 s. Because of the common formation of a reddish coating on many of the crystals (vide infra), it was necessary to scrape off this coating or break the crystal to expose the inside of it to acquire a more accurate elemental analysis.

X-ray Crystallography. Single-crystal X-ray diffraction data for the compounds were collected at room temperature on a Bruker AXS SMART CCD diffractometer. Data processing was then performed using the program SAINT.[10] The structures were refined with the SHELXTL package of programs, using direct methods.[11] Aluminum and silicon sites were distinguished based on bond lengths and elemental analysis (vide infra). Data collection and refinement parameters for representative compounds can be found in Table 2. Atomic positions and occupancy data for these three compounds are listed in Tables 3, 4, and 5. Selected bond length ranges are shown in Table 6. Additional crystallographic data for all compounds are available in the Supporting Information as CIF files.

Magnetic Properties. Magnetic susceptibility measurements were carried out to determine the oxidation state of the rare earth in the europium and ytterbium compounds. Samples were powders ground from single crystals previously analyzed by EDS and X-ray diffraction. A Quantum Design SQUID magnetometer was used to collect data from 3 to 300 K. Variable temperature data were collected at a field of 2000 G. Field dependence data from 0 to 5.5 T were collected at 3 K. Orientational dependence measurements were carried out on single crystals on some compounds. The crystals were mounted on a rotating sample holder, and data were collected with the crystal oriented with its *c*-axis along the magnetic field and again with the *c*-axis perpendicular to the field.

Results and Discussion

Synthesis. The combination of an early rare earth metal, gold, and silicon in excess aluminum resulted in the formation of several quaternary intermetallic compounds with approximate stoichiometries of $REAuAl_2Si$, $REAu_2Al_4Si$, $REAu_3Al_6Si$, and $REAu_4Al_8Si$. Unfortunately, because of their closely related structures, it is difficult to isolate each compound as a pure phase. Instead, the solid product is a mixture of phases; the relative ratios of the structures can be controlled to some extent by adjusting the reactant ratio. A gold-poor reaction mixture (such as a Ce/Au/Al/Si ratio of 1:1:10:5) will favor the formation of $CeAuAl_2Si$ (30% yield, based on Au reactant) and $CeAu_2Al_4Si$ (15% yield, based on Au), with smaller amounts of $CeAu_4Al_8Si$ (5% yield). A gold-rich reaction (1:3:10:2) will promote a higher yield (40%) of $CeAu_4Al_8Si$, but it was not possible to restrict the product formation to a single phase. Choice of the rare earth element adds an additional degree of control over products. As shown in Table 1, the $REAuAl_2Si$ phase only forms with RE = La, Ce, Nd, and Eu; the $REAu_3Al_6Si$ stoichiometry was only found for RE = Nd, Eu, and Yb. Byproducts of these reactions include recrystallized gold and silicon.

The compound $REAuAl_2Si$ crystallizes from the aluminum flux as bevelled rectangles; the other members of the series form as large flat plates. Compounds containing relatively large amounts of gold (such as $REAu_4Al_8Si$) were sometimes coated with a reddish-purple film. This film is poor in aluminum and silicon with an elemental ratio of approximately RE_2Au_7; it is also observed on crystals of the similarly gold-rich ternary intermetallics $REAu_3Al_7$ and $Yb_3Au_7Al_{26}Ti$.[12,13] It is likely due to the slow leaching of surface aluminum during the isolation from the flux in 5 M NaOH. Despite this, the crystals are fairly stable in this solution; they are also stable in dilute acids. The presence of this film is an aid to distinguishing the gold-rich compounds from the other quaternary members of the series in the product (such as $REAuAl_2Si$ and $REAu_2Al_4Si$).

(10) *SAINT*, version 4; Siemens Analytical X-ray Instruments Inc.: Madison, WI, 1995.
(11) Sheldrick, G. M. *SHELXTL, Structure Determination Programs*, version 5.0; Siemens Analytical X-ray Instruments Inc.: Madison, WI, 1995.
(12) Latturner, S. E.; Bilc, D.; Ireland, J.; Kannewurf, C. R.; Mahanti, S. D.; Kanatzidis, M. G. J. *Solid State Chem.* **2003**, *170*, 48–57.
(13) Latturner, S. E.; Kanatzidis, M. G. *Inorg. Chem.* **2004**, *43*, 2–4.

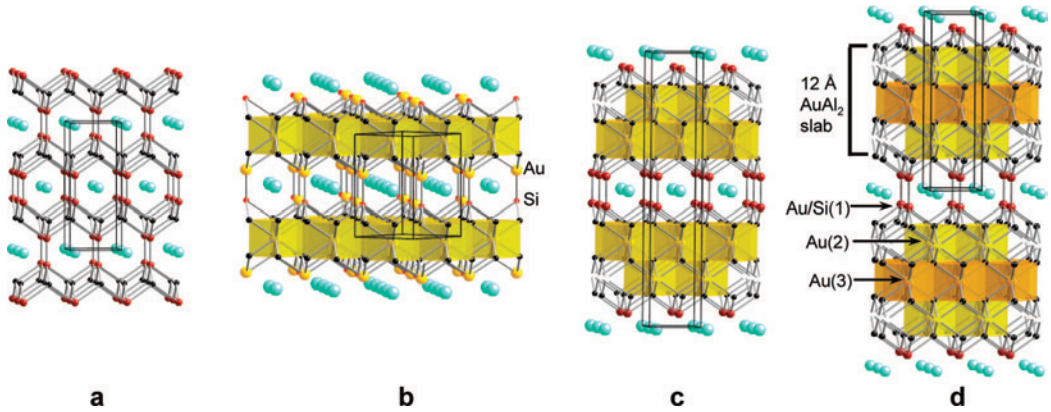

Figure 1. Structures of the four RE$[AuAl_2]_nAl_2(Au_xSi_{1-x})_2$ compounds; blue spheres: rare earth atoms; black spheres: Al atoms; and red spheres: Au/Si mixed site. The antifluorite $AuAl_2$ layer is represented in polyhedral form (yellow spheres: Au). (a) $BaAl_4$ baseline structure of $REAuAl_2Si$. (b) $REAu_2Al_4Si$ structure, with Au and Si ordering producing a supercell; viewed down the [110] direction. (c) $REAu_3Al_6Si$ structure. (d) $REAu_4Al_8Si$ structure; the thick $AuAl_2$ slab is highlighted. There is also a Au/Si ordered supercell of this structure (not shown) with 6 Å × 28 Å *I*4/*mmm* symmetry.

Other synthetic techniques were investigated for these systems. Because of the excess of aluminum in these flux reactions, it can be utilized as a reducing agent toward certain oxides. Using a rare earth oxide precursor is convenient as these compounds are less expensive than elemental rare earths and are also stable in air, making the use of a dry box unnecessary. Reactions were carried out using CeO_2 (Sylvania, 99.9%), with a CeO_2/Au/Al/Si ratio of 1:2:20:5. This did produce the intermetallics $CeAu_4Al_8Si$ and $CeAu_2Al_4Si$, indicating that rare earth oxide reactants can successfully be used to synthesize these materials in aluminum flux. Another synthetic technique that was explored was arc melting a stoichiometric ratio of elements; this was not successful in synthesizing these phases.

Structure. X-ray diffraction studies indicate that all of the compounds formed in these reactions have related structures that comprise a homologous series, RE-$[AuAl_2]_nAl_2(Au_xSi_{1-x})_2$. The tetragonal structures, shown in Figure 1, can be considered as intergrowths of $BaAl_4$-type layers containing the RE atoms and antifluorite-type $AuAl_2$ layers that increase in thickness with *n*. The cell parameters vary regularly with the radius of the rare earth ions (Figure 2), with the exception of the Eu and Yb analogues. This indicates that these ions are likely divalent or mixed valent; magnetic susceptibility measurements were carried out to confirm this (vide infra). Next, we will discuss the $BaAl_4$-type layers and $AuAl_2$ layers separately.

$BaAl_4$-Type Layer. In all four compounds, the rare earth atoms are distributed in a square net in the *ab*-plane, with the distance between them around 4.2–4.3 Å (equivalent to the *a*-axis unit cell parameter for most of the structures). The coordination environment around the RE atoms is equivalent to that of barium in $BaAl_4$. Eight atoms surround this site in a roughly cubic manner, at a distance of 3.2–3.3 Å (see Table 6). In the $BaAl_4$-, $REAu_3Al_6Si$-, and disordered $REAu_2Al_4Si$- and $REAu_4Al_8Si$-type structures, these eight atoms are positioned on one crystallographic site, and its symmetry generated equivalents. Analysis of the X-ray data indicates that this site is occupied by a mixture of gold and a lighter atom, either Al or Si; for all the analogues, the ratio is close to 1:1. The bond lengths from this atom to

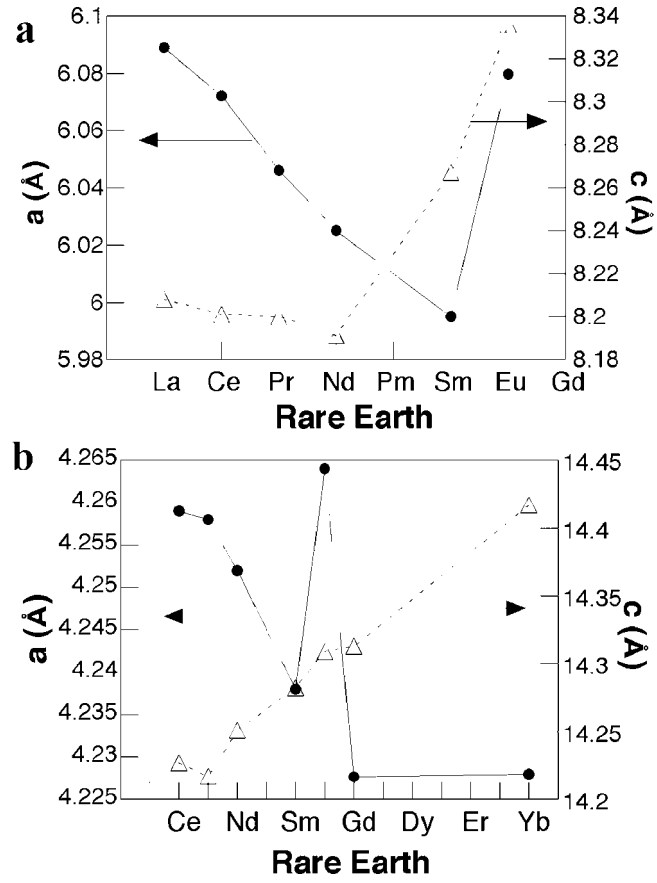

Figure 2. Dependence of unit cell parameters on the size of the RE ion. (a) $REAu_2Al_4Si$ analogues and (b) $REAu_4Al_8Si$ analogues.

neighboring sites include a 2.4–2.5 Å bond to its symmetry-generated equivalent and a 2.5–2.6 Å bond to four aluminum atoms. A mixture of gold and aluminum on this site would be expected to result in longer bonds; it is therefore apparent that the site is occupied by a mixture of Au and Si and is denoted by Au_xSi_{1-x} in the formula for the series (with $x \approx 0.5$ for most of the compounds). This assignment is also supported by electronegativity arguments. Gold and silicon, as the most electronegative atoms in the structure, would be expected to be in close vicinity to the electropositive rare earth ion. The tendency for tetrelides (Si and Ge) to occupy

sites closest to a rare earth element is observed in compounds such as $Tb_2NiAl_4Ge_2$, $SmNiAl_4Si_2$, and $Gd_2PtAl_6Si_4$.[4,14] Mixing of tetrelides and electronegative transition metals on sites closely coordinating a rare earth ion is observed in $Sn_2Ni(Ni_xSi_{1-x})Al_4Si_6$ and $REAuAl_4(Au_xGe_{1-x})$.[4,15] The assignment of gold and silicon to this site in a 1:1 ratio results in the idealized stoichiometries $REAuAl_2Si$, $REAu_3Al_6Si$, and $REAu_4Al_8Si$, which agree with EDS results for these compounds. The slight variations from this ratio determined from the X-ray data—with most compounds showing a slight excess of Si, indicating that there are no Au–Au bonds—are reflected in the unit formulas listed in Table 1.

Two examples are observed where the gold and silicon atoms actually order in this position, producing a superstructure. The disordered substructure for the $REAu_2Al_4Si$ stoichiometry would possess *P4/mmm* symmetry and a unit cell of 4 Å × 8 Å, a structure equivalent to KCu_4S_3.[8] This is seen only for the $EuAu_2Au_4Si$ analogue. In most of the $REAu_2Al_4Si$ compounds, however, ordering of Au and Si in the rare earth coordination sphere results in a superstructure with $a^* = a\sqrt{2}$ and a lower symmetry of *P4/nmm*; this is shown in Figure 1b. This ordering is not absolute; as indicated by the stoichiometries in Table 1 and occupancies listed for the $LaAu_{1.96}Al_4Si_{1.04}$ analogue in Table 3, there is a slight mixing of Si on the gold site and vice versa. Similar ordering is observed for the Sm- and Gd-containing variants of the $REAu_4Al_8Si$ structure. The disordered structure seen for the majority of analogues with this stoichiometry has a unit cell of 4 Å × 14 Å with *P4/mmm* symmetry; ordering of Au and Si produces an *I4/mmm* supercell with $a^* = a\sqrt{2}$ and $c^* = 2c$.[9]

AuAl$_2$ Layers. The rare earth-containing $BaAl_4$-type layers are separated by slabs of the antifluorite structure $AuAl_2$. As in bulk $AuAl_2$, these layers contain gold atoms coordinated by a cube of eight Al atoms and Al atoms tetrahedrally coordinated by gold. The antifluorite slabs in the $RE[AuAl_2]_nAl_2(Au_xSi_{1-x})_2$ series increase in size as n varies from 0 to 3, with a maximum thickness in the $REAu_4Al_8Si$ compounds of around 12 Å. As evidenced in Table 6, the Au–Al bond lengths in the center of the thicker layers approach the value of 2.597 Å seen in bulk $AuAl_2$, varying from this value toward the outer parts of the slabs (near the $BaAl_4$ layers). Because of the regularity in the symmetry and changing size of the $AuAl_2$ layers, according to the rules of the homologous series, it is possible to predict possible new compounds that are higher members[16] (see Scheme 1). For example, a product with $REAu_5Al_{10}Si$ stoichiometry and an *I4/mmm* 4 Å × 35 Å unit cell is predicted as the $n = 4$ member. The same applies for $n = 5$.

This series of quaternary intermetallic compounds bears many similarities to a set of three intermetallic structures resulting from the reaction of the actinide thorium with Au and Si in aluminum flux. The $Th_2(Au_xSi_{1-x})[AuAl_2]_nSi_2$ structures can be considered as intergrowths of $CeNiSi_2$-type and antifluorite $AuAl_2$-type layers.[17] In these tetragonal and orthorhombic structures, layers of thorium atoms are interdigitated by silicon zigzag chains, indicated by the extra Si_2 in the formula for this series of compounds. The resulting $CeNiSi_2$-type coordination environment of thorium is different from that of the rare earth ions in the $RE[AuAl_2]_nAl_2(Au_xSi_{1-x})_2$ series studied in this work. However, both series of compounds feature $AuAl_2$ slabs of varying thickness capped by a mixed occupancy site containing Au or Si, as shown in Figure 3a. The maximum thickness of the $AuAl_2$ slab for both series of compounds is 12 Å, observed in $REAu_4Al_8Si$ and $Th_2Au_5Al_8Si_2$. The variation in Au–Al bond lengths within these slabs shows the same behavior nearly identical to those in bulk $AuAl_2$ in the middle of the slab—and showing variation from this length as the edges of the slab are approached. Another feature of note in the $Th_2(Au_xSi_{1-x})[AuAl_2]_nSi_2$ series is the lack of an $n = 3$ compound. The $AuAl_2$ layer of such a homologue would be identical to that found in $REAu_3Al_6Si$ (Figure 1c), a structure that only forms with Nd, Eu, and Yb. Whether this rarity reflects an inherent instability of this particular $AuAl_2$ fragment is not known.

Scheme 1. Symmetries and Structures of Archetypical $RE[AuAl_2]_nAl_2(Au_xSi_{1-x})_2$ Series Members[a]

Formula	*n*	*symmetry*	*cell size*
$REAuAl_2Si$	0	*I4/mmm*	4.2 × 10 Å
$REAu_2Al_4Si$	1	*P4/mmm*	4.2 × 8.2 Å
$REAu_3Al_6Si$	2	*I4/mmm*	4.2 × 22.5 Å
$REAu_4Al_8Si$	3	*P4/mmm*	4.2 × 14.3 Å
($REAu_5Al_{10}Si$	4	*I4/mmm*	4.2 × 35 Å)
($REAu_6Al_{12}Si$	5	*P4/mmm*	4.2 × 20.5 Å)

[a] Au/Si mixed site is roughly 50% Au and 50% Si in all cases ($x = 0.5$); this results in the idealized formulas shown.

Evidence for the role of silicon in aluminum flux in promoting the formation of $AuAl_2$ layers can be found in early work on Au–Al interfaces on silicon devices. A number of research groups determined that the presence of silicon at the Au–Al junction accelerates the formation of $AuAl_2$ at the expense of other intermetallics such as Au_2Al and Au_4Al. This process incidentally results in an electrical and mechanical degradation at the junction, sometimes referred to as the "purple plague" due to the violet color of $AuAl_2$.[7] Similar behavior appears to be at work when gold and silicon are combined with a rare earth or an actinide (Th) in liquid aluminum. It should be noted that in the absence of silicon, ternary RE/Au/Al ternary intermetallics form that do not show the antifluorite $AuAl_2$ structural motif. These phases include $REAu_3Al_7$ with a complex rhombohedral structure, $RE_3Au_2Al_9$, and the $REAuAl_3$ and $REAu_2Al_2$ compounds with the $BaAl_4$-type structure.[12,18] The latter phases have a

(14) Latturner, S. E.; Bilc, D.; Mahanti, S. D.; Kanatzidis, M. G. *Inorg. Chem.* **2003**, *42*, 7959–7966.
(15) Wu, X. U.; Kanatzidis, M. G. *J. Solid State Chem.* **2005**, *178*, 3233–3242.
(16) (a) Mrotzek, A.; Kanatzidis, M. G. *Acc. Chem. Res.* **2003**, *36*, 111–119. (b) Kanatzidis, M. G. *Acc. Chem. Res.* **2005**, *38*, 359–368.
(17) Latturner, S. E.; Bilc, D.; Mahanti, S. D.; Kanatzidis, M. G. *Chem. Mater.* **2002**, *14*, 1695–1705.
(18) (a) Miller, G. *Eur. J. Inorg. Chem.* **1998**, 523–536. (b) Nordell, K. J.; Miller, G. J. *Angew. Chem., Int. Ed. Engl.* **1997**, *36*, 2008–2010. (c) Hulliger, F. *J. Alloys Compd.* **1995**, *218*, 255–258. (d) Hulliger, F.; Nissen, H. U.; Wessicken, R. *J. Alloys Compd.* **1994**, *206*, 263–266. (e) Hulliger, F. *J. Alloys Compd.* **1993**, *200*, 75–78.

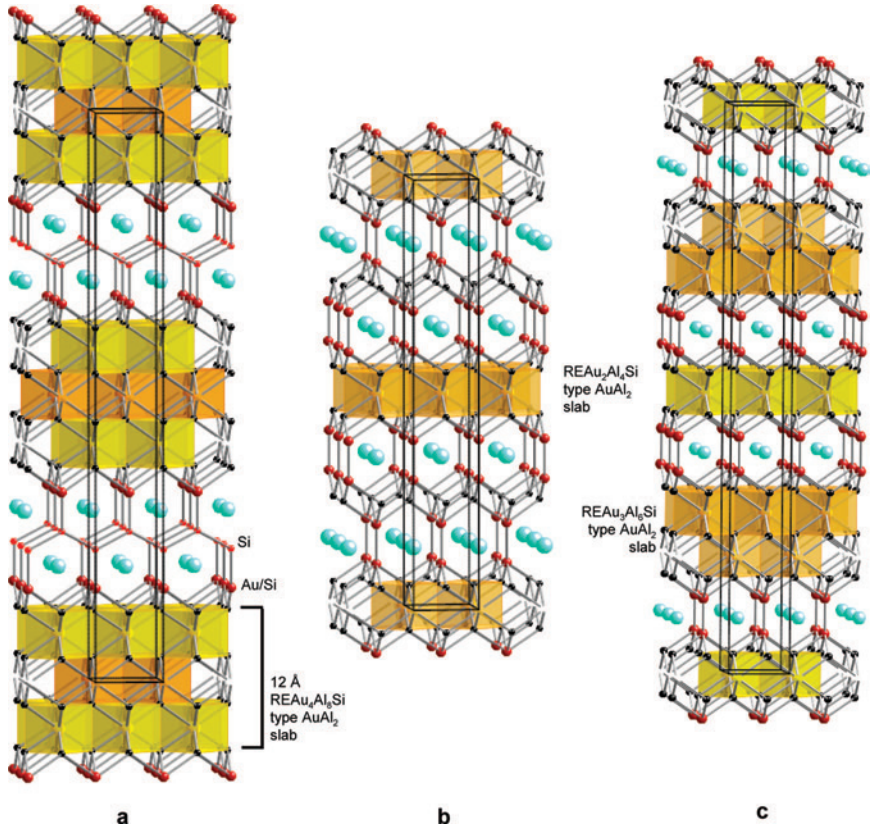

Figure 3. Structure of $Th_2Au_5Al_8Si_2$ and two intergrowth structures, showing the common occurrence of various $AuAl_2$ layers. Blue spheres: rare earth or Th atoms; black spheres: Al atoms; and dark red spheres: Au/Si mixed site. The antifluorite $AuAl_2$ layer is represented in polyhedral form (yellow spheres: Au). (a) $Th_2Au_5Al_8Si_2$ can be described as an intergrowth of $CeNiSi_2$ layers (with a Si zigzag chain) and 12 Å thick $AuAl_2$ slabs. (b) $Eu_2Au_{2.25}Al_6Si_{2.75}$, with the Ce_2NiGa_{10} structure, combines the $AuAl_2$ layers found in $REAuAl_2Si$ and $REAu_2Al_4Si$. (c) $Gd_2Au_{4.93}Al_{10}Si_{2.07}$ contains $AuAl_2$ slabs from $REAu_2Al_4Si$ and $REAu_3Al_6Si$.

trivially small fragment of $AuAl_2$, consisting of a square net of aluminum atoms capped on alternating sides by gold atoms (Figure 1a). However, thicker $AuAl_2$ slabs such as those found in $REAu_4Al_8Si$ and $Th_2Au_5Al_8Si_2$ are not found in gold-containing aluminide intermetallics in the absence of silicon.

Several compounds that can be described as intergrowths of thin antifluorite structure slabs and thick $BaAl_4$-type slabs were reported in the early 1980s by Grin et al.[19] Combinations of La, Ni, and Ga in a variety of ratios were arc melted, and the resulting phases were investigated. $LaGa_6Ni_{1-x}$ was found to have a tetragonal KCu_4S_3 structure type (the disordered variant of the $REAu_2Al_4Si$ structure, Figure 1b). La_2NiGa_{10} was found to have a new structure with two kinds of small antifluorite slabs (a RE/Au/Al/Si analogue of this structure was found in our study, which is discussed in the next section; see Figure 3b). In both these gallide structures, the $BaAl_4$-type layers are the dominant structural motif; no thick antifluorite-type $NiGa_2$ layers are observed. This could be due to the small amount of Ni used in the reactions, although higher ratios of nickel do not seem to result in the formation of antifluorite slabs. Both in aluminum and in gallium systems, nickel-rich compounds such as YNi_3Al_9 form trigonal or hexagonal structures with nickel in a stuffed arsenic-type environment.[20] The same kinds of Ni-containing building blocks are formed upon the addition of silicon, for instance, in $RE_{0.67}Ni_2Al_4Si$ and related gallium analogues.[21] A comparison of the title compounds to these and other RE/late transition metal/aluminum/silicon intermetallics indicates that gold and silicon have an idiosyncratic behavior when combined in aluminum flux with an early rare earth element. This may be related to the strong interactions between these elements, as seen in the exceptionally deep eutectic observed in the Au–Si phase diagram.[22]

The geometry of the $AuAl_2$ slabs may be crucial in determining what rare earth ions can be incorporated into the $RE[AuAl_2]_nAl_2(Au_xSi_{1-x})_2$ structures. These compounds only form with RE = La– to Gd and Yb. These early rare earths have larger radii than the later rare earths. The ytterbium analogues appear to be anomalies, but the radius of divalent Yb is 0.93 Å, comparable to that of Gd^{3+}.[23] The thorium atoms in the $Th_2(Au_xSi_{1-x})[AuAl_2]_nSi_2$ series also fit into this size regime; the Th^{4+} ionic radius is similar to

(19) (a) Grin, Y. N.; Yarmolyuk, Y. P.; Rozhdestvenskaya, I. V.; Gladyshevskii, E. I. *Sov. Phys. Crystallogr.* **1982**, *27*, 418–419. (b) Yarmolyuk, Y. P.; Grin, Y. N.; Rozhdestvenskaya, I. V.; Usov, O. A.; Kuzmin, A. M.; Bruskov, V. A.; Gladyshevskii, E. I. *Sov. Phys. Crystallogr.* **1982**, *27*, 599–600.

(20) Gladyshevskii, R. E.; Cenzual, K.; Flack, H. D.; Parthe, E. *Acta Crystallogr., Sect. B: Struct. Sci.* **1993**, *49*, 468–474.

(21) Zhuravleva, M. A.; Chen, X. Z.; Wang, X. P.; Schultz, A. J.; Ireland, J.; Kannewurf, C. K.; Kanatzidis, M. G. *Chem. Mater.* **2002**, *14*, 3066–3081.

(22) Massalski, T. B.; Okamoto, H. *Binary Alloy Phase Diagrams*, 2nd ed.; ASM International: Material Park, OH, 1990.

(23) Shannon, R. D. *Acta Crystallogr., Sect. A: Found. Crystallogr.* **1976**, *32*, 751.

that of Pr^{3+}. Considering the $AuAl_2$ structure, the cubic unit cell edge of bulk antifluorite $AuAl_2$ (5.97 Å) corresponds to the diagonal of a 4.22 Å tetragonal cell ($a^* = \sqrt{2}a$). Inspection of the *a* cell parameter in Table 1 shows a range from 4.225 to 4.31 Å for all the RE[$AuAl_2$]$_n$Al$_2$(Au$_x$Si$_{1-x}$)$_2$ structures. Also notable is the fact that the orthorhombic structure of $Th_2Au_5Al_8Si_2$ has cell parameters in this range (a = 4.2612(8) Å and c = 4.2487(8) Å). This requirement to fit the rare earth ion into a pocket of the $AuAl_2$ structure may be a reason for the lack of late rare earth $REAu_4Al_8Si$ analogues.

Intergrowth Compounds. The presence of a variety of $AuAl_2$ slab synthons forming in the aluminum flux reaction medium is highlighted by the isolation of a number of more complex intergrowth structures that contain more than one kind of $AuAl_2$ layer. $Eu_2Au_{2.25}Al_6Si_{2.75}$, shown in Figure 3b, has a La_2NiGa_{10} structure type and contains two kinds of $AuAl_2$ layers. It can be described as a combination of the $REAuAl_2Si$ and $REAu_2Al_4Si$ structures. Likewise, the $Gd_2Au_5Al_{10}Si_2$ structure (Figure 3c) can be considered as an intergrowth of the $REAu_2Al_4Si$ and $REAu_3Al_6Si$ types. These results point to the possibility that careful study of a crystal of a RE[$AuAl_2$]$_n$Al$_2$(Au$_x$Si$_{1-x}$)$_2$ compound with TEM would reveal the presence of misfit layers or more complex intergrowth patterns, where an ordered array of one type of $AuAl_2$ slabs is disrupted by randomly placed $AuAl_2$ slabs of a different size.

Magnetic Behavior of Europium and Ytterbium Analogues. The synthesis of $YbAu_{2.91}Al_6Si_{1.09}$ and $YbAu_{3.86}Al_8Si_{1.14}$ was unexpected since this class of compounds was thought to form only with early rare earth ions. The deviation of the unit cell parameters from the normal trend in $REAu_4Al_8Si$ (Figure 2) indicated that the Yb ions might be divalent or mixed valent, and magnetic susceptibility measurements were carried out to confirm this. The data for these Yb compounds ($YbAu_{3.86}Al_8Si_{1.14}$ data shown in Figure 4) show nearly temperature independent behavior at high temperatures with a low molar susceptibility of 2×10^{-3} emu/mol. This is consistent with diamagnetic Yb^{2+} ions in a metallic compound exhibiting Pauli paramagnetic behavior. However, at lower temperatures, an increase in the susceptibility indicates the presence of paramagnetic Yb^{3+} ions. As the temperature is lowered, the contraction of the lattice may favor the formation of Yb^{3+} ions by the promotion of an f-electron to the conduction band, forming a mixed valent state.[24] The application of X-ray absorption near edge spectroscopy (XANES) to probe the appearance of Yb^{3+} species would be interesting.

All four RE[$AuAl_2$]$_n$Al$_2$(Au$_x$Si$_{1-x}$)$_2$ structures have europium analogues. All of the europium compounds show slight variations in behavior as compared to those containing other rare earth ions. The yields of the four structures were unusual, with $EuAu_{0.6}Al_3Si_{0.4}$ being the most abundant and $EuAu_{1.95}Al_4Si_{1.05}$ the least abundant at all reactant ratios we examined. $EuAu_{1.95}Al_4Si_{1.05}$ is also the only $REAu_2Al_4Si$ analogue that did not feature an ordering of Au and Si atoms

(24) Varma, C. M. *Rev. Mod. Phys.* **1976**, *48*, 219–238.

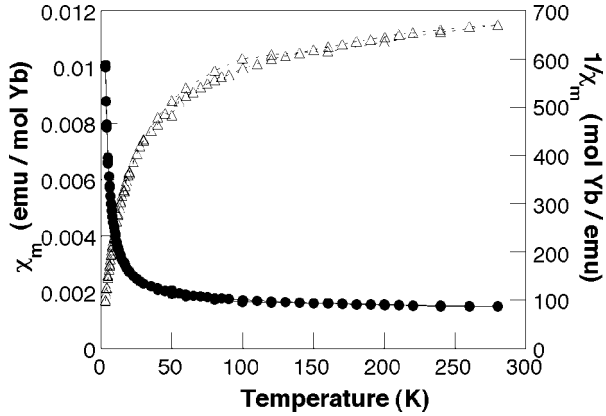

Figure 4. Magnetic susceptibility data for $YbAu_{3.86}Al_8Si_{1.14}$. Solid circles are χ_m data; open triangles are $1/\chi_m$ data.

to form the *P4/nmm* supercell. The gold contents are also anomalous, as confirmed by SEM-EDS and X-ray diffraction; the mixed Au_xSi_{1-x} sites of $EuAu_{2.58}Al_6Si_{1.42}$ and $EuAu_{3.68}Al_8Si_{1.32}$ are low in Au, and the $BaAl_4$-type $EuAu_{0.6}Al_3Si_{0.4}$ is low in Au and Si. The decrease in the normal amount of Au could be due to a charge effect (with the divalent Eu^{2+} ion needing less electronegative neighbors as compared to the RE^{3+} ions of other analogues) or a size effect (with the larger Eu^{2+} needing smaller atoms around it).

Eu is divalent in all four systems as indicated by the anomalies in unit cell parameters; this is confirmed by magnetic susceptibility data shown in Figure 5. The Eu systems show Curie–Weiss behavior at high temperatures, with a fit of the data from 70 to 300 K indicating a magnetic moment of 7.5–8.5 μ_B/Eu ion, in agreement with the theoretical value of 7.94 μ_B predicted for Eu^{2+}. $EuAu_{0.6}Al_3Si_{0.4}$ undergoes ferromagnetic ordering at 10 K, as evidenced by the steep increase in the molar susceptibility and the kink in the inverse susceptibility data. Instead of leveling off in the magnetically ordered state, the χ_m data begin to drop at 5 K, indicating a possible switch to an antiferromagnetically ordered state. The other three europium compounds order antiferromagnetically: $EuAu_{1.95}Al_6Si_{2.05}$ at 14 K and $EuAu_{2.58}Al_6Si_{1.42}$ and $EuAu_{3.68}Al_8Si_{1.32}$ at 11 K.

Measurements on single crystals of $EuAu_{2.58}Al_6Si_{1.42}$ and $EuAu_{3.68}Al_8Si_{1.32}$ show identical behavior in terms of orientation, both in temperature dependence and in field dependence. Data for $EuAu_{2.58}Al_6Si_{1.42}$ are shown in Figure 5c,d. The spins on the Eu^{2+} ions are obviously oriented along the *c*-axis when ordered. This is shown by the sharp drop off of χ_m when the crystal is positioned with its *c*-axis parallel to the magnetic field and the leveling off of χ_m when the crystal's *c*-axis is perpendicular to the field. $EuAu_{2.58}Al_6Si_{1.42}$ and $EuAu_{3.68}Al_8Si_{1.32}$ also show identical field dependence behavior at 3 K for the two different crystal orientations. There is a metamagnetic transition at around 25 000 G observed when a crystal is positioned with its *c*-axis (and therefore the antiferromagnetically coupled spins) oriented parallel to the magnetic field.

It appears that increasing the thickness of the $AuAl_2$ layer past a certain point may convert the magnetic behavior of

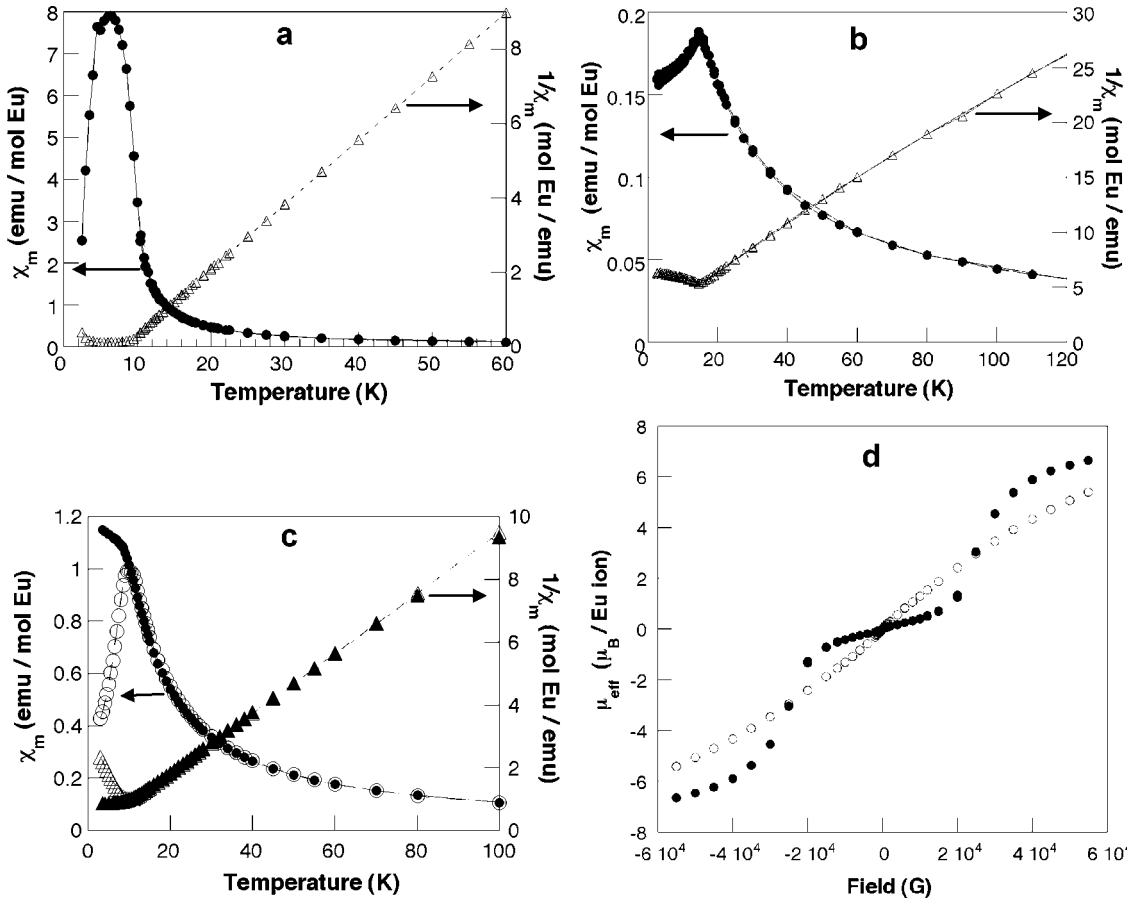

Figure 5. Magnetic susceptibility data for Eu/Au/Al/Si compounds. (a) $EuAu_{0.6}Al_3Si_{0.4}$ isotropic susceptibility data. (b) $EuAu_{1.95}Al_4Si_{1.05}$ isotropic susceptibility data. (c) $EuAu_{2.58}Al_6Si_{1.42}$ single-crystal susceptibility data; open symbols represent data collected with the crystal *c*-axis oriented parallel to the applied field, and solid symbols represent data collected with the *c*-axis perpendicular to the field. (d) $EuAu_{2.58}Al_6Si_{1.42}$ magnetization data; filled symbols represent data collected with the crystal *c*-axis oriented parallel to the applied field, and solid symbols represent data collected with the *c*-axis perpendicular to the field.

the Eu/Au/Al/Si compounds from 3-D to 2-D. The fact that $EuAu_{2.58}Al_6Si_{1.42}$ and $EuAu_{3.68}Al_8Si_{1.32}$ show identical susceptibility behavior indicates that the 2-D europium-containing layers (the $BaAl_4$ layers) are not interacting with each other; the Eu^{2+} ions within each layer couple antiferromagnetically, but they do not couple to adjacent layers of Eu^{2+} ions. Without a thick $AuAl_2$ slab as a barrier between the Eu layers, they can interact in three dimensions; this may be the cause of the FM ordering observed in the $BaAl_4$-type $EuAu_{0.6}Al_3Si_{0.4}$. The exact $AuAl_2$ thickness needed to convert the 3-D ferromagnetic system of $EuAu_{0.6}Al_3Si_{0.4}$ to a 2-D antiferromagnetic system is not clear; due to the low yield and small crystals of $EuAu_{1.95}Al_6Si_{2.05}$, this could not be studied in more detail. However, this compound does show antiferromagnetic ordering at a somewhat similar temperature to the analogues with thicker $AuAl_2$ layers, an indication that 2-D behavior might be appearing. These four $Eu[AuAl_2]_nAl_2(Au_xSi_{1-x})_2$ homologues can be viewed as Eu/$AuAl_2$/Eu magnetic layer heterostructures, analogous to the Fe/Cr superlattices studied for magnetoresistance materials.[25] The initial studies on such samples indicated that iron layers separated by a critical thickness of a nonmagnetic interlayer become exchange decoupled and behave as a 2-D system.[26] Similar behavior may be occurring for $EuAu_{2.58}Al_6Si_{1.42}$ and $EuAu_{3.68}Al_8Si_{1.32}$.

Conclusion

Molten aluminum is a rich medium for new synthetic chemistry. This behavior is also found in gallium and indium, which make this group of triels a powerful set of solvents for intermetallic materials discovery.[2,27] The interaction of silicon and gold in aluminum in the presence of rare earth elements is strong and appears to promote the growth of 2-D $AuAl_2$ slabs, driving the formation of the homologous series $RE[AuAl_2]_nAl_2(Au_xSi_{1-x})_2$, which is related to the previously described $Th_2(Au_xSi_{1-x})[AuAl_2]_nSi_2$ series. Investigations into replacing Si with Ge in these reactions have produced

(25) Grunberg, P. *Acta Mater.* **2000**, *48*, 239–251.

(26) Grunberg, P.; Schreiber, R.; Pang, Y.; Brodsky, M. B.; Sowers, H. *Phys. Rev. Lett.* **1986**, *57*, 2442–2445.

(27) (a) Chondroudi, M.; Balasubramanian, M.; Welp, U.; Kowk, W. K.; Kanatzidis, M. G. *Chem. Mater.* **2007**, *19*, 4769–4775. (b) Salvador, J. R.; Kanatzidis, M. G. *Inorg. Chem.* **2006**, *45*, 7091–7099. (c) Zhuravleva, M. A.; Bilc, D.; Pcionek, R. J.; Mahanti, S. D.; Kanatzidis, M. G. *Inorg. Chem.* **2005**, *44*, 2177–2188. (d) Salvador, J. R.; Malliakas, C.; Gour, J. R.; Kanatzidis, M. G. *Chem. Mater.* **2005**, *17*, 1636–1645. (e) Zhuravleva, M. A.; Kanatzidis, M. G. *Z. Naturforsch B.* **2003**, *58*, 649–657. (f) Salvador, J. R.; Gour, J. R.; Bilc, D.; Mahanti, S. D; Kanatzidis, M. G. *Inorg. Chem.* **2004**, *43*, 1403–1410.

compounds with the KCu_4S_3 structure (e.g., $EuAuAl_4(-Au_{1-x}Ge_x)_2$)[15] but not with the thicker $AuAl_2$ slabs characteristic of silicide structures $REAu_3Al_6Si$, $REAu_4Al_8Si$, and $Th_2Au_5Al_8Si_2$. The layered nature of these structures may lead to highly anisotropic properties. Additional studies are planned, as well as further investigations into the possibility of a mixed valence in the Yb compounds using band structure calculations and XANES.

Acknowledgment. This work made use of the SEM facilities of the Center for Electron Optics at Michigan State University. Financial support from the Department of Energy (Grant DE-FG02-07ER46356 to Northwestern University) is gratefully acknowledged.

Supporting Information Available: Crystallographic collection parameters and tables of atomic positions and isotropic thermal parameters for intergrowth structures and ordered superstructures and further crystallographic data in CIF format. This material is available free of charge via the Internet at http://pubs.acs.org.

IC701799Z